NUMERICAL PREDICTION OF SHIP RESISTANCE AND SQUAT IN CONFINED WATERS

F. LINDE[*†], A. OUAHSINE[*], N. HUYBRECHTS[*†] and P. SERGENT[†]

[*]Sorbonne Universités, Université de Technologie de Compiègne
Laboratoire Roberval, UMR-CNRS 7337
Centre de Recherches de Royallieu, CS 60319, 60203 Compiègne Cedex, FRANCE
e-mail: florian.linde@developpement-durable.gouv.fr

[†]DTecEMF, CEREMA
134 rue de Beauvais, CS 60039, 60280 Margny Lès Compiègne, France

Key words: Ship Resistance, Ship Squat, Restricted Waterways, Computation Fluid Dynamics, Free Surface Flow, Fluid-Structure Interaction.

Abstract. Accurate prediction of hydrodynamic forces opposing a ship displacement in restricted waterways is necessary in order to improve energy efficiency of inland transport. When a ship moves in restricted waterways, a significant increase in ship squat (combination of sinkage and trim) and resistance occurs compared to a movement in open waters. In this paper, a 3D numerical model based on fluid-structure coupling is presented and used to investigate the effect of limited water depth and channel width on ship resistance and squat.

1 INTRODUCTION

When a ship moves in restricted waterways the water in front of its bow is pushed away creating an increase in pressure and a void appears behind the stern creating a decrease in pressure. Due to the reduction of the section where the water can flow, the flow around the ship is also accelerated. The increase in the water speed under the ship causes a decrease in pressure and as a result, a vertical force is applied on the ship making it drop vertically down in the water. The uneven pressure distribution along the ship hull creates a moment along the transverse axis which leads the ship to trim by the bow or the stern. These phenomena have a direct impact on ship resistance: the acceleration of the flow around the hull of the ship causes an increase of friction and ship sinkage increases the quantity of water that the ship needs to push in order to move forward.

In the past, ship resistance in open waters has been studied in towing tank with ship models. The results of those studies have been used to develop empirical models for open waters [1]. However, over the past few years, with the increase in computing power and

development of new numerical methods, there has been a growing interest in Computational Fluid Dynamics (CFD) techniques and its application to ship hydrodynamic and open water ship resistance. Stern et al. [2] reviewed the progress made over the last ten year in CFD applied to ship hydrodynamics and The Gothenburg 2010 Workshop on Numerical Hydrodynamics [3] gathered the results of 33 groups on 18 cases and concluded that the mean error for all computed resistance cases was practically zero.

In shallow and restricted water, near Schijf-limiting speed [4], squat effects become significant and ship resistance increases dramatically [5]. Briggs et al. [6] reviewed PIANC empirical formulas for predicting squat in canals and in restricted and open channels. Ship squat has also been studied with numerical methods often based on Boundary Elemement Method [7], Tucks theory [8], CFD [9] and mathematical models [10]. However, most of these methods do not model ship sinkage and as result the flow modification induced by the squat phenomenon is not accounted for. Some empirical model have been developed in order to predict ship resistance in shallow water [11] and restricted waterways [12]. These methods use the open water formulas with a correcting factor for ship's speed. Few numerical studies of ship resistance in shallow water and even less in restricted waters have been done. Most of them are based on the resolution of the Reynolds Averaged Navier-Stokes (RANS) equations associated with a phase transport model (Volume Of Fluid method, Level-Set) [13]. To the knowledge of the author, none of those studies include ship squat effect on the resistance. In general, ship resistance and ship squat are studied separately. On one hand, numerical models predicting ship squat solve non-viscous fluid equations (Euler) and thus cannot evaluate ship resistance; on the other hand, numerical ship resistance models do not take ship squat into account in their calculations. Therefore, this study aims to develop a ship resistance prediction model allowing to take ship squat and viscous effects into account.

2 THEORETICAL APPROACH

2.1 Fluid equations

The fluid is considered incompressible. The governing equations for the viscous free surface flow problem are the RANS equations:

$$\frac{\partial u_i}{\partial x_i} = 0 \tag{1}$$

$$\frac{\partial \rho \overline{u}_i}{\partial t} + \frac{\partial}{\partial x_j}(\rho \overline{u}_i \overline{u}_j) = \frac{\partial \overline{p}}{\partial x_i} + \frac{\partial}{\partial x_j}(\mu \frac{\partial \overline{u}_i}{\partial x_j} - \rho \overline{u'_i u'_j}) \tag{2}$$

where x_i is the ith (i=1,2,3) component of the fixed coordinate system, ρ is the fluid density, $\overline{u}_i$ and $\overline{p}$ are the mean velocity and pressure, μ is the fluid dynamic viscosity and $-\rho \overline{u'_i u'_j}$ is the Reynolds stress. To solve the closure problem, the SST $\kappa - \omega$ turbulence model has been used.

2.2 Solid equations

The ship's hull is modelled as a rigid body. The movement of the ship is governed by the rigid body equations of motion written at the body's centre of mass:

$$m\overrightarrow{a_G} = \sum \overrightarrow{F} \tag{3}$$

$$\frac{d}{dt}(I_G \cdot \overrightarrow{\omega_G}) = \sum \overrightarrow{M_G} \tag{4}$$

where m is the mass of the body, $\overrightarrow{a_G}$ is the body acceleration, $\sum \overrightarrow{F}$ is the sum of the external forces, I_G is the moment of inertia tensor, $\overrightarrow{\omega_G}$ is the angular velocity and $\sum \overrightarrow{M_G}$ is the sum of the applied torques.

3 NUMERICAL SOLUTION
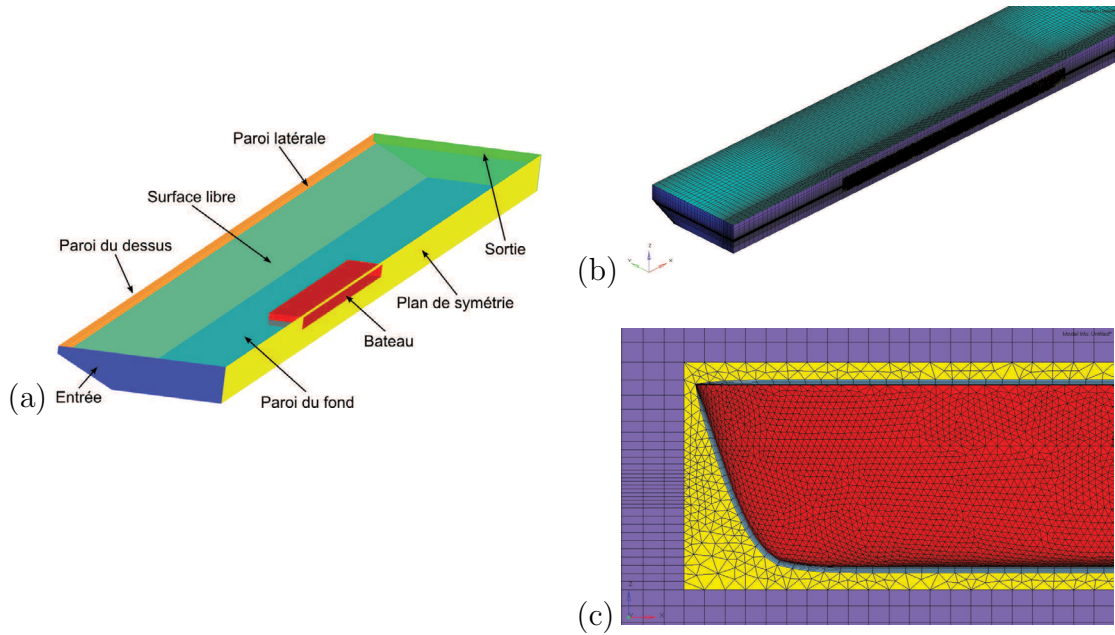
3.1 Fluid equations

Figure 1: Geometric domain and associated mesh: (a) computational domain with boundaries, (b) meshed domain with higher density on free surface and around ship hull, (c) box with unstructured and boundary layer mesh

Fluid equations (eqs. (1) and (2)) are solved by using Ansys Fluent CFD code. This solver uses finite volume method to discretise the domain into a finite set of control volumes on which the general conservation (transport) equations are solved. The pressure-velocity coupling is solved by using the SIMPLE algorithm. The VOF method is used

in order to simulate the free surface and ship waves [14, 15]. The 2nd order Upwind scheme is used for the dicretization of the convective terms. Pressure conditions were specified at the open boundaries (inlet and outlet); wall conditions with no slip were used for the bottom, the side and the ship hull; and symmetry conditions were set for the symmetry plane and the top. A structured-unstructured hybrid mesh consisting of about 1.3 millions cell was generated for the whole domain. Structured elements are used on the whole domain except around the hull where an unstructured mesh was generated in order to remesh the domain during the actualisation of the ship position. A prismatic boundary layer mesh has also been used around the ship hull. Figure 1 below shows the geometric domain and associated mesh.

3.2 Solid equations

In order to find the ship equilibrium position, the rigid body motion equations (eqs. (3) and (4)) are usually solved in time until the body reach equilibrium. As a result, this method requires to model the transient state and ship oscillations around the hull. However, this study only takes interest in the equilibrium position and steady state. Moreover, here, only ship sinkage is modelled. Therefore, the equilibrium position is defined as follows:

$$F_z = (\overrightarrow{P} + \overrightarrow{F_f}) \cdot \overrightarrow{e_z} = (\iint_S \boldsymbol{\sigma} \cdot \overrightarrow{n} dS - m \overrightarrow{g}) \cdot \overrightarrow{e_z} = 0 \tag{5}$$

where F_z is the projection of forces on $\overrightarrow{e_z}$ axis, m is the mass of the ship, $\overrightarrow{g}$ is the gravitational acceleration, $\overrightarrow{F_f}$ is the force from the fluid acting on the hull of the shp which can be decomposed as viscous and pressure forces, $\boldsymbol{\sigma} = \boldsymbol{\tau} - p\mathbf{I}$ is the stress tensor, $\boldsymbol{\tau}$ is the shear stress, p is the pressure, $\mathbf{I}$ is the identity matrix, $\overrightarrow{n}$ is the normal vector to the ship's hull and S is the wetted surface of the ship's hull. Newton's method was used in order to solve this nonlinear equation. Let z^N be the vertical position of the gravity center and $F_z(z^N)$ the sum of the vertical forces at the Nth iteration of the Newton algorithm. The iteration of the algorithm is given by:

$$z^{N+1} = z^N - \frac{F_z(z^N)}{F_z'(z^N)} \tag{6}$$

As there is no analytical expression for F_z, its derivative is calculated using finite difference.

3.3 Fluid-structure interaction (FSI)

The coupling between fluid and solid models is as follows: solving the fluid equations allows to evaluate the forces acting on the hull, which are then used as an input in order to iterate Newton's method and calculate the displacement of the ship; and finally the fluid equations are solved again. This iterative process is presented in fig. 2.
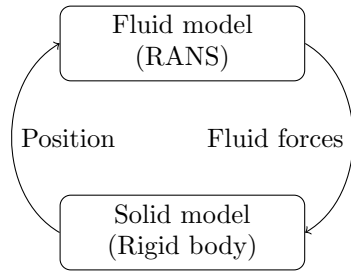
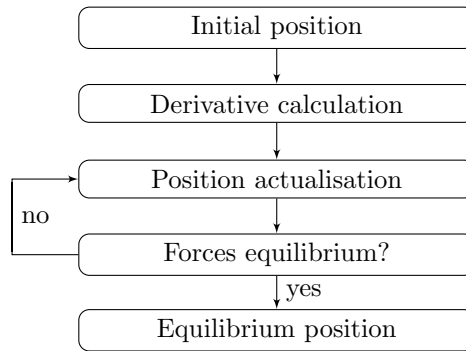**Figure 2**: Fluid-structure interaction

Figure 3: Numerical resolution process

As the derivative of F_z is calculated by finite difference, it is necessary to evaluate the forces at two positions: z^N and $z^N + dz_0$, where dz_0 is a small increment of the vertical position. Moreover, after each actualisation of the position, the solution of the fluid problem is disturbed and n iterative resolutions of the fluid equations are required to reach a new stable solution and change the ship's position again. As a result, calculating the derivative of the forces can be time consuming and in order to make the calculations faster, a quasi-Newton method has been used, where the derivative is calculated only once and kept constant during all the iterative process. A study comparing the speed convergence of the two methods has been carried out and it has been shown that the quasi-Newton method converges faster but it needs more iterations N compared to the Newton algorithm. Figure 3 describes the numerical resolution process.

4 EXPERIMENTAL DATA

In 2013, in collaboration with the University of Liege (Belgium), an experimental work was carried out at the ANAST towing tank in order to validate the numerical model. In these experiments a 135 m (full size) inland vessel was used at 1/25 scale. A wide range of parameters were tested such as channel width (W), channel depth (H) and ship draft (T). The boat was free to sink and trim and forces and moments acting on the ship as well as sinkage and trim were recorded.

In this paper, the effect of limited water depth and channel width on ship resistance and squat is investigated. According to ITTC87 [16], some of the parameters to consider in order to estimate the nature and level of restriction for waterways are:

- water depth to draught ratio $\frac{H}{T}$, if $\frac{H}{T} < 4$, there is an influence of the bottom on the flow around the hull;

- water width to ship breadth (B) ratio $\frac{W}{B}$, if $\frac{W}{B} < 4$, the flow around the hull changes;

- canal section (A_C) to midship section (A_B) $\frac{A_C}{A_B}$ ratio, a general restriction of the waterway starts when $\frac{A_C}{A_B} < 15$.
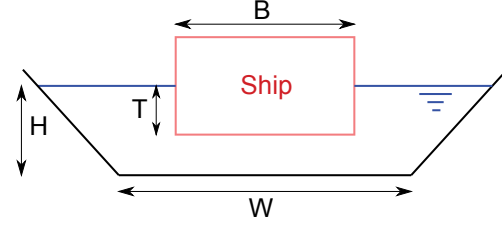

Figure 4: Schematic representation of the model and waterway geometric parameters

Table 1 sums up the different configurations for which the experimental data were compared to the numerical results as well as the values for the restriction parameters described above.

Table 1: Modelled configurations and corresponding parameters

Conf.	H [m]	T [m]	W [m]	$\frac{H}{T}$ [-]	$\frac{W}{B}$ [-]	$\frac{A_C}{A_B}$ [-]	V [m/s]	V_L [m/s]
C1	0.18	0.10	0.72	1.80	1.58	4.26	0.11-0.51	0.58
C2	0.18	0.10	1.44	1.80	3.16	7.11	0.22-0.56	0.74
C3	0.18	0.10	2.88	1.80	6.32	12.79	0.33-0.67	0.88
C4	0.24	0.10	2.88	2.40	6.32	17.68	0.44-0.89	1.10
C5	0.18	0.04	2.88	4.50	6.32	31.97	0.44-0.89	1.04

V_L=Schijf limiting speed [4]

5 RESULTS AND DISCUSSION

5.1 Mesh convergence study

A grid convergence study was carried out for the configuration 3 using a fine grid and coarsening it two times by a factor $\sqrt{2}$ in all directions. Table 2 shows the number of elements as well as the change in drag (C_D) and lift (C_L) coefficients.

Table 2: Dependence of drag (C_D) and lift (C_L) coefficients on grid density (configuration 3, V=0.67 m/s)

Grid	No. Elements	C_D [-]	C_L [-]	$\frac{C_D}{C_{Dfine}}$ [%]	$\frac{C_L}{C_{Lfine}}$ [%]
Coarse	0.34 M	0.310	2.847	106.07	99.53
Medium	0.85 M	0.296	2.856	101.31	99.85
Fine	2.23 M	0.293	2.860	100	100

Table 2 shows that the grid sensitivity between the medium and fine grid is very limited : the change for the lift coefficient is less than 1% and around 1.3% for the drag coefficient. As a result, an intermediate grid between the medium and fine grid was chosen to maintain an affordable computational cost. This grid was generated by keeping similar mesh parameters outside the ship box and increasing mesh density inside ship box which resulted in 1.3 M elements.

5.2 Quasi-Newton algorithm convergence

Figure 5 below illustrates the convergence of the quasi-Newton algorithm for configuration 3 at speed $V = 0.57$ m/s.
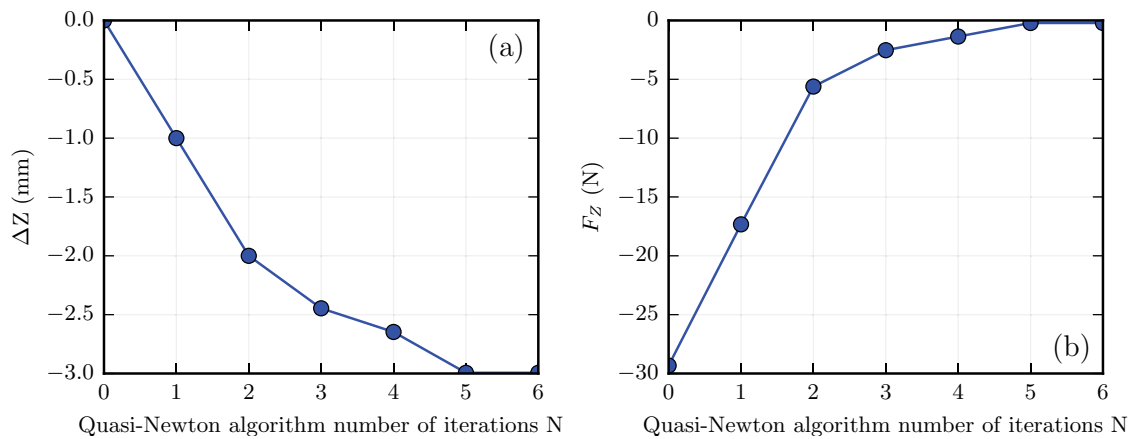

Figure 5: Quasi-Newton algorithm convergence for configuration 1 at speed $V = 0.57$ m/s : change in (a) ship sinkage ΔZ and (b) vertical forces F_Z

In this case, the equilibrium position is reached after 5 iterations of the algorithm. The stopping criteria is set for $F_Z < 0.5$ N and in order to prevent any remeshing error (negative volume) the maximum displacement is set to 1mm. It is worth noticing that this algorithm can easily be extended to two degrees of freedom (in order to take trim into account for instance) by introducing the Jacobian matrix. Linde et al. (2014) [17] studied the influence of taking sinkage into account on the numerical results but in the experiments carried out at the University of Liege, the trim angle was so low that it had no impact on ship resistance and ship sinkage was the predominant factor. As a result, only ship sinkage is modelled in this study.

5.3 Restricted-water effect and comparison with experimental data

Figure 6 compares numerical results with experimental data for the 5 configurations listed in table 2.
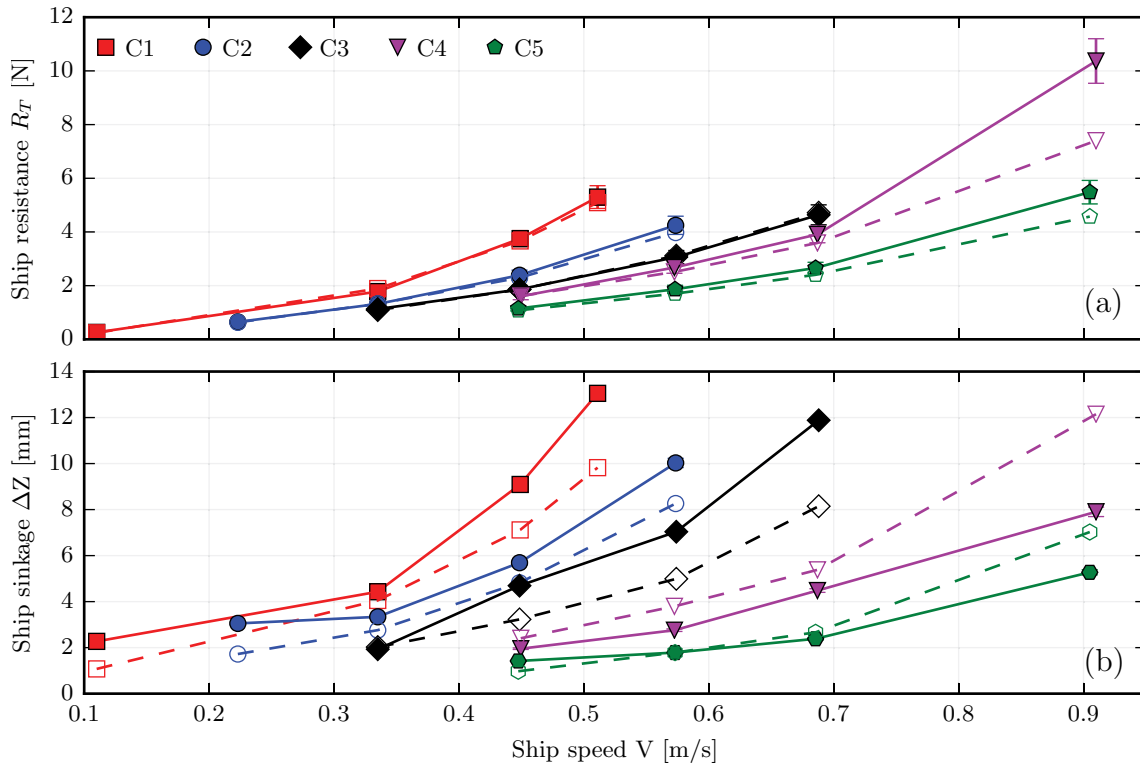
Figure 6: Restricted-water effect: comparison between numerical (full line with filled markers) and experimental (dashed line with empty markers) results for conf. 1-5. Change in (a) ship resistance R_T and (b) ship sinkage ΔZ against ship speed V.

From fig. 6, it can be seen that as restriction increases (i.e $\frac{A_C}{A_B}$ ratio decreases - C5 to C1) ship resistance and sinkage increase. For instance, for $V = 0.44 \ m/s$, ship resistance and sinkage in configuration 1 are respectively 1.9 and 4.7 times higher than in configuration 4. The comparison between numerical and experimental results shows that for ship speed up to 0.7 m/s the predicted resistance is in a very good agreement with the experimental data. For ship sinkage, the numerical results show the same trend as the experiment however, there seems to be an offset. This could be explained by the potential error made when measuring the initial draft during the experiment as the uncertainty on the measure is $\pm$ 1 mm. For the ship speed of 0.9 m/s the numerical model overestimates the sinkage and underestimate the resistance. It is possible that for this speed the model is not able to reproduce correctly the pressure field around the ship hull therefore underestimating vertical and horizontal pressure forces. This prediction error is currently under investigation. So far, the influence of parameters such as mesh density, boundary conditions or turbulence model have been tested, but none of them had an impact on the error.

5.4 Influence of ship sinkage on the resistance prediction error

Figure 7 shows the predicted resistance with sinkage without sinkage as well as the experimental data for configuration 1,2 and 3.
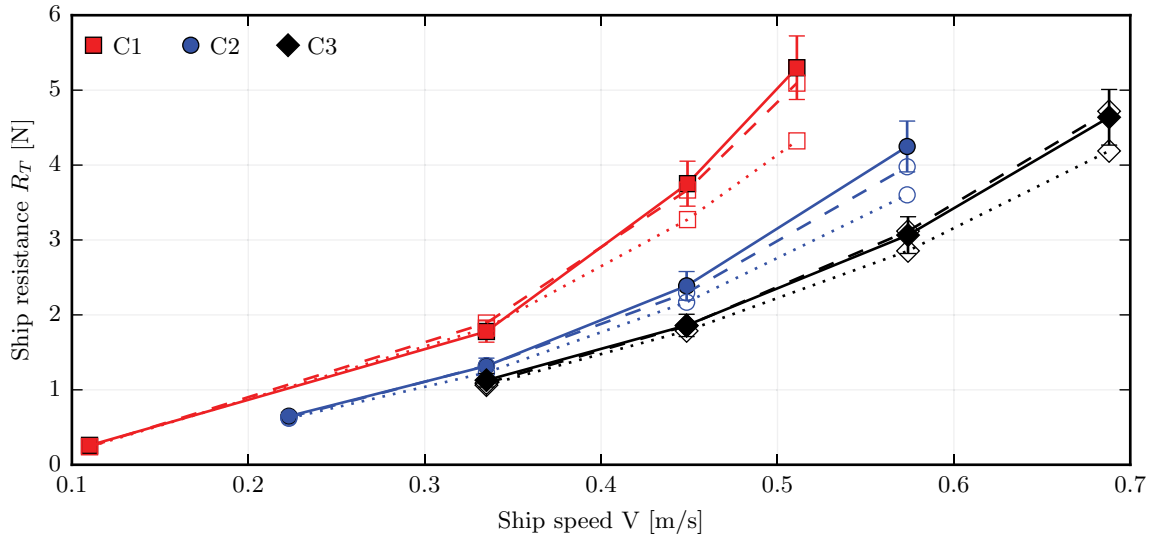

Figure 7: Comparison between the predicted resistance with sinkage (dashed line, empty markers) and without sinkage (dotted line, empty markers) as well as the experimental data (full line with filled markers) for configuration 1,2 and 3.

Figure 7 shows that up to a speed of 0.33 m/s, the predicted resistance with or without sinkage does not differ much. However, above that speed, there is a gap between the measured data and predicted resistance without sinkage; meanwhile the plot of the resistance with sinkage remains very close to the experimental data. This observation is sustained by the calculated prediction error: the error with sinkage is almost always smaller than that without sinkage. Moreover, for those three configurations, the maximum error is 6.3 % with sinkage whereas it reaches 18.4 % without sinkage. Moreover, the calculated increase in ship resistance due to ship sinkage can be very significant: it reaches a maximum value of 18% for configuration 1 at 0.51 m/s. It can also be seen that the prediction error without sinkage significantly increases with the speed and the restriction of the water, which is not the case for the predicted resistance with sinkage. Those facts highlight the significance of taking ship sinkage into account in order to accurately predict ship resistance in restricted waterways.

5.5 Influence of restriction parameters on ship resistance increase

In order to study if the depth restriction $(\frac{H}{T})$ or the width restriction $(\frac{W}{B})$ has more effect on resistance, two sets of simulations were carried out. Starting from a reference configuration with a rectangular channel, in one case the water depth was decreased while

the channel width remained constant, and the opposite was done in the other case. The increase in ship resistance is then compared with the reference resistance R_{Tref} calculated for the initial configuration. The use of a rectangular channel ensures the similarity of the definition of the two ratio and the reference configuration was chosen so that both have the same value ($\frac{H}{T} = \frac{W}{B} = 5$, equal restriction). For this study, the ship described in section 4 was used, the draught remained constant and two speeds were tested (0.4 m/s and 0.6 m/s). The two set-ups are described in table 3 and illustrated in fig. 8.

Table 3: Modelled set-ups used to study the influence of restriction parameters

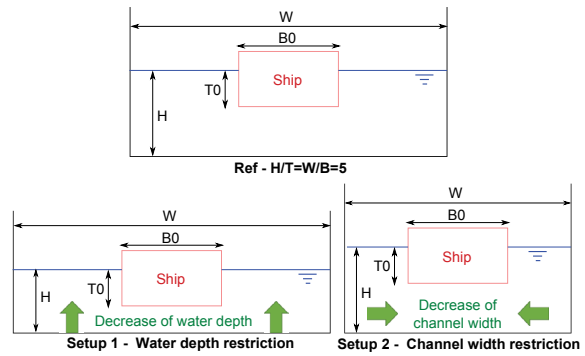| Setup	H [m]	W [m]	$\frac{H}{T}$ [-]	$\frac{W}{B}$ [-]
Ref	0.5	2.28	5	5
S1	0.15-0.4	2.28	1.5-4	5
S2	0.5	0.68-1.82	5	1.5-4

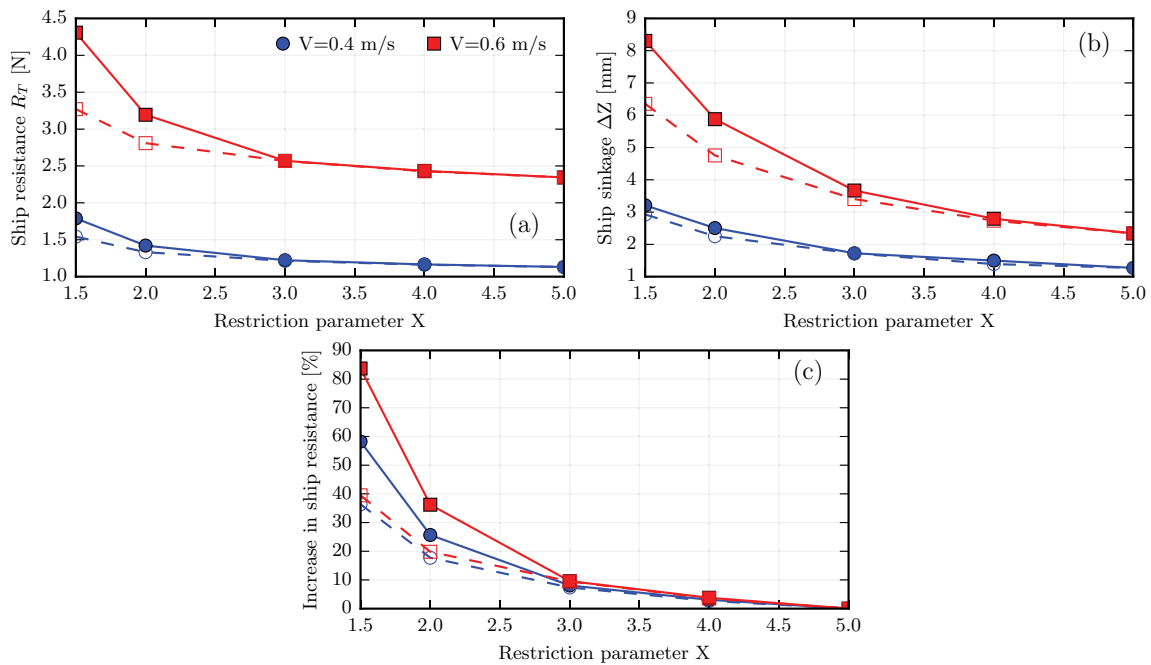**Figure 8**: Illustration of the two tested set-ups

Figure 9: Evolution of (a) ship resistance, (b) ship sinkage and (c) increase of ship resistance against restriction parameter X ($X = \frac{H}{T}$ for set-up 1 (full line with filled markers) and $X = \frac{W}{B}$ for set-up 2 (dashed line with empty markers)

Figure 9 shows the evolution of ship resistance (fig. 9 (a)) and ship sinkage (fig. 9 (b)) as well as the increase in ship resistance $\frac{R_T(X) - R_{Tref}}{R_{Tref}}$ (fig. 9 (c)) due to depth restriction in set-up 1 and channel width restriction in set-up 2. Figure 9 (a) and fig. 9 (b) show that significant differences in ship resistance and sinkage between the water depth and channel width restriction begin to appear when the restriction parameter is inferior to 3. This difference also increases with the increase in ship velocity. It can also be seen that for a given speed, the resistance and sinkage start to rise for a value of the restriction parameter below 4, which is in agreement with the findings of the ITTC87 mentioned in section 4. It is clear from fig. 9 (c) that water depth restriction has more influence on ship resistance increase than channel width restriction: for the 0.6 m/s velocity, the increase amounts to 84 % for $\frac{H}{T} = 1.5$ against 39 % for $\frac{W}{B} = 1.5$. This can be explained by the fact that ship sinkage is less sensitive to vertical restriction than horizontal restriction. Indeed, under the hull, the increase of flow velocity and the pressure drop will be less impacted by a decrease of channel width than a decrease of water depth.

6   CONCLUSIONS

The numerical model presented in this article allows to calculate ship resistance in restricted waterways by taking ship sinkage into account. The use of a Newtonian method in order to find the equilibrium position allows to skip the transient state. Moreover, this method can easily be extended to two degrees of freedom by using a Jacobian matrix. The comparison with experimental data has shown that predicted resistance and sinkage were in good agreement for velocities below 0.7 m/s but discrepancies appeared for the highest tested velocity (0.9 m/s). Taking ship sinkage into account allowed to significantly reduce the prediction error. Finally, the model was used to study the influence of channel width and water depth restriction. The results showed that in the case of water depth restriction, ship sinkage was more significant which resulted in higher ship resistance increase.

REFERENCES

[1] Holtrop, J. and Mennen, G.G. An approximate power prediction method. *International Shipbuilding Progress* (1982) **19**:166–170.

[2] Stern, F. *et al.* Computational ship hydrodynamics: nowadays and way forward. *International Shipbuilding Progress* (2013) **60**:3–105.

[3] Larsson, S., Stern, F. and Visonneau, CFD in ship hydrodynamics—results of the Gothenburg 2010 workshop. *Marine 2011* (2013) 237–259.

[4] Schijf, J.B. Influence on the Form and Dimensions of the Cross-Section of the Canal, of the Form, of the Speed and the Propulsion System of Vessels. *XVIIth PIANC* (1949).

[5] Constantine, T. The behaviour of ship moving in restricted waterways. *ICE Proceedings* (1961) **19**:549–562.

[6] Briggs, M.J., Vantorre, M., Uliczka, K., Debaillon, P. Prediction of squat for underkeel clearance. *Handbook of Coastal and Ocean Engineering* (2013).

[7] Härting, A., Laupichler, A., Reinking, J. Considerations on the squat of unevenly trimmed ships. *Ocean Engineering* (2009) **36**:193–201.

[8] Gourlay, T. Slender-body methods for predicting ship squat. *Ocean Engineering* (2008) **35**:191–200.

[9] Debaillon, P. Numerical investigation to predict ship squat. *Journal of Ship Research* (2010) **54**:133–140.

[10] Lataire, E., Vantorre, M., Delefortrie, G. A prediction method for squat in restricted and unrestricted rectangular fairways. *Ocean Engineering* (2012) **55**:71–80.

[11] Schlichting, O. Ship Resistance in Water of Limited Depth-Resistance of Sea–Going Vessels in Shallow Water. *Jahrbuch der STG* (1934) **35**:127–148.

[12] Geerts, S., Verwerft, B., Vantorre, M., Van Rompuy, F., *et al.* Improving the efficiency of small inland vessels. *European Inland Waterway Navigation Conference* (2010).

[13] Toxopeus, S. L. Viscous-flow calculations for KVLCC2 in deep and shallow water. *Marine 2011* (2013) 151–169.

[14] JI, S.C., Ouahsine, A., Smaoui, H., Sergent, P. 3-D numerical simulation of convoy-generated waves in a restricted waterway. *Journal of Hydrodynamics, Ser. B* (2012) **24**:420–429.

[15] JI, S.C., Ouahsine, A., Smaoui, H., Sergent, P. 3D Numerical modeling of Sediment resuspension induced by the compounding effects of ship-generated waves and the ship propeller. *Journal of Engineering Mechanics* (2013) **140 (6)**:04014034.

[16] Resistance and flow committee. Report of the resistance and flow committee. *18th International Towing Tank Conference* (1987).

[17] Linde, F., Ouahsine, A., Huybrechts, N., Sergent, P. Effet de la pronfondeur limitée sur la résistance à l'avancement et l'enfoncement dynamique d'une barge fluviale. *14èmes Journées de l'Hydrodynamique* (2014).